

Nafion-Graphene Nanocomposite *in situ* Plated Bismuth-film Electrodes on Pencil Graphite Substrates for the Determination of Trace Heavy Metals by Anodic Stripping Voltammetry

Keagan Pokpas, Nazeem Jahed*, Oluwakemi Tovide, Priscilla G. Baker and Emmanuel I. Iwuoha

SensorLab, Department of Chemistry, University of the Western Cape, Bellville 7535, South Africa.

*E-mail: njahed@uwc.ac.za

Received: 1 April 2014 / Accepted: 12 May 2014 / Published: 16 June 2014

The use of disposable and inexpensive pencil graphite rods, modified with a Nafion-graphene nanocomposite, in conjunction with an *in situ* plated bismuth-film is reported as electrochemical sensor for the determination of trace amounts of Zn^{2+} , Cd^{2+} and Pb^{2+} in tap water samples. Synthesised graphene was characterised using electron microscopy, FTIR and Raman spectroscopy. The Nafion-graphene nanocomposite pencil graphite bismuth-film electrode (NG-PG-BiE) exhibited superior detection capabilities as a result of increased surface area, electron conductivity and binding properties of the NG-Bi film. The instrumental parameters associated with the simultaneous determination of target metals namely, bismuth-film concentration, deposition potential, deposition time and rotation speed were investigated and optimized. Relative standard deviation (RSD %) for the oxidation peaks were calculated to be within the 1.5 – 3.3 % range of for all three target metal ions. The NG-PG-BiE showed detection limits of $0.17 \mu g L^{-1}$, $0.09 \mu g L^{-1}$ and $0.13 \mu g L^{-1}$ for Zn^{2+} , Cd^{2+} and Pb^{2+} respectively, at a deposition time of 120 seconds. Finally, the electroanalytical sensor was successfully applied towards the determination of target metal ions in tap water samples below the USEPA standards of $5 mg L^{-1}$, $5 \mu g L^{-1}$ and $15 \mu g L^{-1}$ for Zn^{2+} , Cd^{2+} and Pb^{2+} respectively.

Keywords: Pencil Graphite, Nafion-graphene Nanocomposite, Bismuth-film Electrode, Anodic Stripping Voltammetry, Heavy Metal

1. INTRODUCTION

Electrochemical techniques, focusing around stripping analysis has garnered widespread attention as a convenient technique for a variety of analysis types [1]. Anodic stripping voltammetry (ASV) is one such method at the forefront of trace metal analysis due to its high sensitivity and multi-elemental analysis capability [2, 3]. Bismuth-film electrodes (BiE) have been sought out as alternatives

to the commonly used toxic mercury electrodes [4]. The formation of “fused” alloys between bismuth and heavy metals [5] together with, good sensitivity and resolution [6] yield electrodes which offer results comparable to those obtained with mercury electrodes. *In situ* plating [7], *ex situ* plating [8] and the modification of electrodes using a bismuth precursor, such as Bi_2O_3 [9] are common methods of bismuth electrode preparation in existence today.

Pencil graphite (PG) has gained popularity as electrode substrate material for chemical and biosensors for example, the determination of trace metals [10, 11], DNA and RNA [12] and, uric acid in urine and blood samples [13]. The attractive features of PG which distinguishes it from other solid electrode materials, including the common glassy-carbon and gold electrodes (GCE and GE) are, its good conductivity, fewer pretreatment steps, low cost, low background current and large scale availability.

Surface-active substances which adsorb onto the working electrode during analysis impede the electrode activity and its performance [14,15] and is a major downfall to the stripping voltammetric process. Conducting polymers and binders can alleviate these interferences [16]. Coating pencil graphite electrodes with Nafion, a perfluorinated ionomer, has shown to increase the detection sensitivity and alleviate the interferences from surfactants at bismuth film electrodes [17]. The perfluorinated ionomer containing negatively charged sulfonic groups has found to be useful as a proton-conducting membrane material for fuel cells and electrochemical applications [18,19]. The Teflon like hydrophobic backbone with its highly hydrophilic ionisable sulfonic groups is responsible for its excellent chemical stability and ionic conductivity [20].

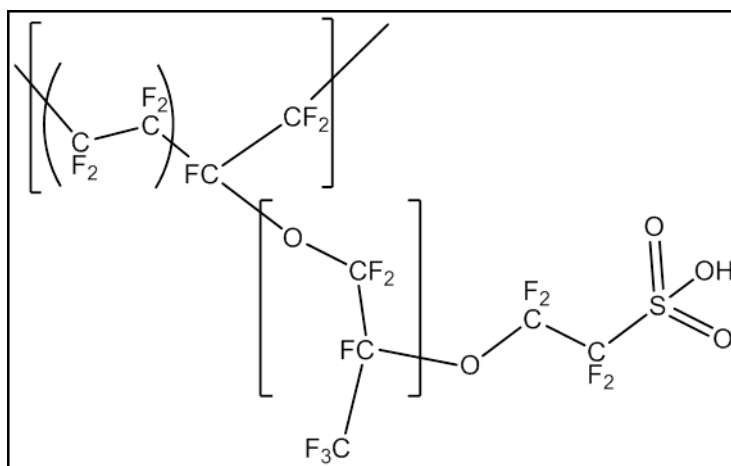


Figure 1.1. 2D Graphic Representation of the Nafion Structure

The unique ion-exchange, discriminative and biocompatibility properties have made Nafion-films useful for the modification of electrode surfaces. The polar side chain of Nafion allows for carbon nanotubes (CNTs) and Graphene to be easily suspended in solutions of Nafion in phosphate buffer and alcohols [21] prior to their deposition or casting onto electrode surfaces.

Modifying carbon based electrodes with graphene or reduced graphene oxide has attracted lots of attention since its discovery. Graphene’s intrinsic physiochemical properties (high surface area,

excellent conductivity, high mechanical strength and ease of functionalization and mass production) make it a perfect platform for a wide range of applications [22]. Graphene-based electrochemical sensors have been employed as chemical sensors in environmental analysis particularly for heavy metal determinations. Li et al. and Willemse et al. reported on Nafion-graphene composite films at the bismuth-film and mercury film for determining Zn^{2+} , Cd^{2+} , Cu^{2+} and Pb^{2+} using DPSV and SWASV, respectively [23, 24]. These works showed improved sensitivity due to the increased surface area and better conductivity as a consequence of the inclusion of graphene when compared to the work performed by Kefala et al. and Demetriades et al. at Nafion-modified, bismuth-film pencil electrodes for Pb and Zn and Pb, Cd and Zn determination using SWASV [25, 26]. The above mentioned graphene-based electrodes exhibit superior detection properties over their carbon nanotube [27, 28] and graphite nanofiber [29] counterparts. Gong et al. reported on a Hg^{2+} sensor with graphene and gold nanoparticles with detection limits as low as 6 parts per trillion (ppt). The sensor inhibits the interference from other heavy metal ions such as Cu^{2+} , Cr^{3+} , Co^{2+} , Fe^{3+} and Zn^{2+} [30] and further supports the use of nanocomposites for enhanced detection capabilities.

Previously, our research group has made use of binder-free [31] as well as Nafion-modified graphene at mercury-film electrodes [24]. Nafion, which acts as a binding agent and ion-exchanger has shown to improve the sensitivity of electrodes towards heavy metal detection [24, 32]. Furthermore, we have reported on the use of the disposable pencil graphite substrate at the less toxic bismuth-film electrodes using electrochemically reduced graphene oxide (EG-PG-BiE).

In this work we report our findings on an inexpensive, disposable pencil graphite electrode modified with a Nafion-graphene nanocomposite and an *in situ* plated bismuth-film for the determination of Zn^{2+} , Cd^{2+} and Pb^{2+} in water samples by SWASV.

2. EXPERIMENTAL PROCEDURE

2.1. Chemicals and Reagents

All chemicals used in this study were analytical reagent grade and used without further purification. Standard stock solutions ($1,000\text{ mg L}^{-1}$, atomic absorption standard solution) were obtained from Sigma-Aldrich and diluted as required.

Acetate buffer (0.1 M, pH 4.6) was used as supporting electrolyte and prepared by mixing glacial acetic acid (CH_3COOH) and sodium acetate (NaOH) followed by diluting the solution with ultra-pure distilled water (Millipore). A pH meter (Metrohm 827 pH Lab.) was calibrated using pH 4 and pH 7 calibration buffer solutions and, then used to verify the pH of the acetate buffer (supporting electrolyte) solution.

Nafion (5 % (w/v)) solution in a mixture of water and lower alcohols was purchased from Aldrich. Diluted solutions (0.2 %) were prepared by diluting 200 μL of 5 wt. % Nafion with 5 mL ethanol in Eppendorf tubes.

Standard solutions were prepared in polyethylene vials in order to limit absorption onto the inner walls of the vial. Atomic absorption stock solutions of Zn^{2+} , Cd^{2+} and Pb^{2+} (1000 ppm) were diluted with 0.01 M HCl.

2.2. Nafion-Graphene Preparation

Graphene oxide was prepared by a modified Hummer's method [33] as reported in our previous work [34]. The synthesised graphene oxide (100 mg) was dispersed in 100 mL of ultra-pure distilled water in a 250 mL round-bottom flask by ultrasonication for 1 hr. Following the ultrasonication, 200 mg NaBH_4 was added and stirred for 30 min. The resulting solution was allowed to cool to room temperature before refluxing at 135 °C for 3 hrs. Once cooled, the synthesis yields a 100 mL graphene in water solution. Separation of aqueous layer from the black solid was then performed by centrifugation. The graphene produced was dried at 60 °C for 3 days in a vacuum oven.

0.25 wt. % NG solutions were prepared by mixing 0.2 % Nafion solution with appropriate amounts of graphene powder followed by ultrasonication for 1 hour.

2.3. Apparatus

Voltammetric measurements were performed using a 797 VA COMPUTRACE instrument (Metrohm, Switzerland) interfaced with a personal computer. The voltammetric cell consisted of a 20 mL glass compartment equipped with an Ag/AgCl (saturated KCl) reference electrode and platinum wire counter electrode. The working electrodes used consisted of PG-BiE, N-PG-BiE and NG-PG-BiEs. All experiments were carried out at ambient temperature.

Fourier Transform Infrared (FT-IR) spectra were recorded using a (Perkin Elmer Spectrum 100) coupled to an Attenuated Total Reflectance (ATR) sample holder. FT-IR was used to obtain information and confirmation on graphene oxide. Scanning Electron Microscopy (SEM) measurements were performed using a LEO 1450 SEM 30 kV instrument equipped with Electronic Data System (EDS) and Windows Deployment Services (WDS); images were taken using the secondary electron detector. The samples were dried in a vacuum oven and deposited on the silicon grid surface before SEM observations. Raman spectroscopy was obtained using a Dilor XY Raman spectrometer with a Coherent Innova 300 Argon laser with a 514.5 nm laser excitation.

The pencil graphite rods (Pentel, HB of 0.5 mm in diameter and 6 cm in length) were purchased from the local book store. A plastic syringe served as a holder into which the pencil rod was inserted exposing 1 cm of the rod tip at one end of the syringe. In order to establish electrical connection with the potentiostat a copper wire was attached to the other end of the pencil rod and passed through the top of the syringe. To achieve accurate and reproducible results in quantitative analysis impeccable electrode hygiene was applied. The pencil graphite electrodes were thoroughly cleaned before each use in a simple reproducible manner. A small quantity of ethanol was placed onto soft tissue paper and the surface of the electrode gently wiped followed by thorough rinsing with ultra-

pure water. Successive dipping of the PGE in a 6 M HNO₃ solution and rinsing with ultra-pure water followed [34].

2.4. Nafion-Graphene Pencil Graphite Electrode (NG-PGE) Preparation

Each pencil graphite electrode surface was electrochemically pre-treated by applying a potential of +1.4V for 30 s in the blank supporting electrolyte (0.1 M acetate buffer solution (ABS) pH 4.6) without stirring in order to increase the hydrophilic properties of the electrode surface through the introduction of oxygenated functionalities during oxidative cleaning as demonstrated in the work by Levent et al [35]. The pre-treated pencil graphite electrodes were immersed in vials containing Nafion-graphene (NG) solution for 5 min and air dried allowing for the evaporation of solvent. This process was repeated three times to produce uniformly coated NG-PGEs.

2.5. Procedure for SWASV analyses

A reduction potential (-1.4 V) was applied to the prepared working electrodes with constant stirring for 120 s in 10 mL solutions of acetate buffer (0.1 M, pH 4.6), 10 μ L of Bi³⁺ stock solution (1000 μ g mL⁻¹) and target metal ions. After a brief rest period (10 seconds) the potential was scanned from -1.4 V to +0.3 V by applying a square-wave waveform to the NG-PGE. At the end of the scan the NG-PGE was electrochemically cleaned from the residual metals by applying a potential of 30 s at +0.3 V, with stirring.

3. RESULTS AND DISCUSSIONS

3.1. Characterization of Graphene

Selected characterization of the synthesised graphene is shown below.

3.1.1. Fourier Transformed Infrared Spectroscopy (FT-IR)

Previous research has shown the dispersal of a variety of oxygen containing functionalities namely, hydroxyl, ethers, epoxides, carbonyl and carboxylic groups [34, 36, 37] along the graphene oxide surface. Figure 3.1 shows the Fourier transformed infrared (FT-IR) spectra of graphite, graphene oxide and graphene. As expected, graphite exhibits no significant characteristic IR features. However, for GO, the following characteristic infrared peaks appear namely, the O-H stretching vibration at 3117 cm⁻¹, the C=O stretching vibration at 1760 cm⁻¹ [38] and aromatic C=C stretching vibration at 1589 cm⁻¹ [37]. The peak at 1401 cm⁻¹ is associated with the bending C-O-H vibration [37], while the peaks at 1260 cm⁻¹ [36] and 1026 cm⁻¹ are due to the C-O stretching vibration occurring in epoxides and alcohols [38] within the graphite structure. Upon reduction using NaBH₄ as reducing agent, a

considerable decrease or complete removal of the above mentioned oxygen containing functionalities is noted demonstrating that all or most of the oxygen have been removed.

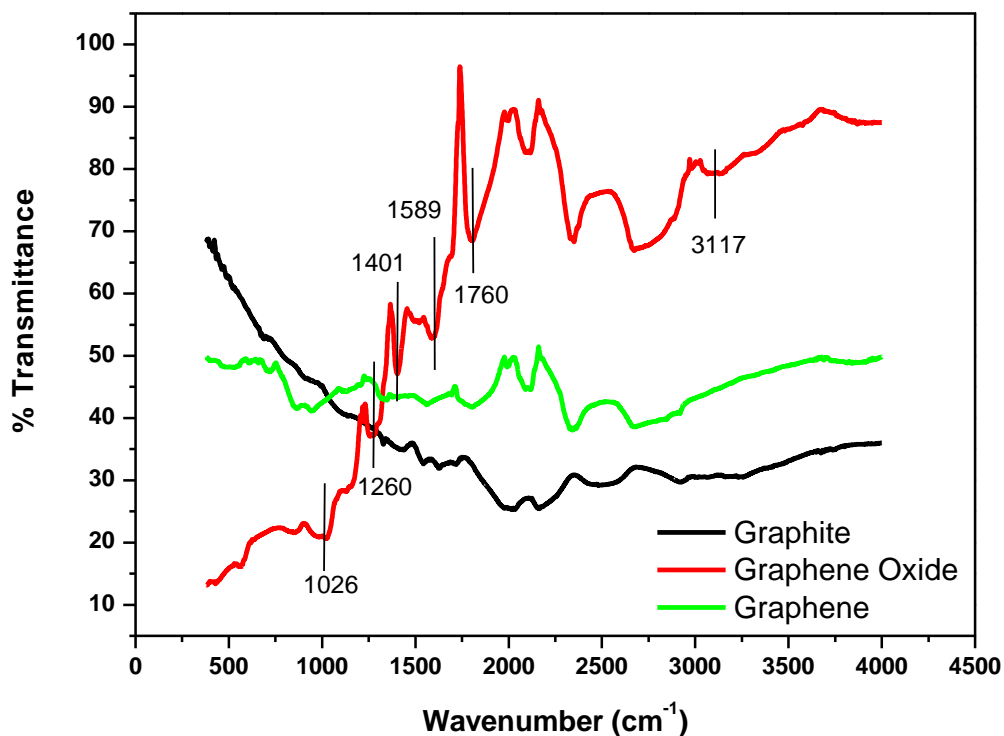


Figure 3.1. FT-IR spectra of Graphite, Graphene Oxide (GO) and Graphene

3.1.2. Raman Spectroscopy

The change in structure, after the chemical transformation, from pure graphite to graphene oxide and graphene was investigated by Raman spectroscopy and represented by Figures 3.2 (a), (b) and (c), respectively. The Raman spectrum for graphite in Figure 3.2 (a) reveals a strong G band at 1575 cm^{-1} , a significantly weaker D band at 1350 cm^{-1} and a moderate 2D band at 2721 cm^{-1} . The G band occurs as a consequence of the symmetry which allows first order scattering of the E_{2g} mode (of sp^3 hybridized carbon atoms) to occur in the neatly ordered graphite structure [39]. The ratio of the intensities of the D and G bands (I_D/I_G), used as a measure of disorder or defects within the structure [40, 41] was calculated as 0.25 for graphite, demonstrating the highly ordered structure.

Graphene oxide [Figure 3.2 (b)] on the other hand shows a significant decrease, broadening and Raman shift to 1600 cm^{-1} for the G band while the D band at 1360 cm^{-1} is considerably larger than in Figure 3.2 (a). This increase is attributed to the reduction in size of the in-plane sp^2 domains caused by the insertion of the epoxy, carboxyl, carbonyl and hydroxyl groups between the individual layers of the graphite [42]. A calculated I_D/I_G ratio of 0.975 was obtained, depicting an increase in structural disorder.

The Raman spectrum of graphene [Figure 3.2 (c)] includes the D peak located at 1345 cm^{-1} , G peak at 1589 cm^{-1} and 2D peak at 2867 cm^{-1} . The D band is attributed to the disorder or defects within the graphene structure or as a result of edge effects [43, 44]. The G band arises due to in-plane vibration of the sp^2 carbon atoms. The 2D band appears at almost double the frequency of the D band and originates from second order Raman scattering processes. An increase in I_D/I_G ratio from 0.975, for GO to 1.17 for graphene was observed.

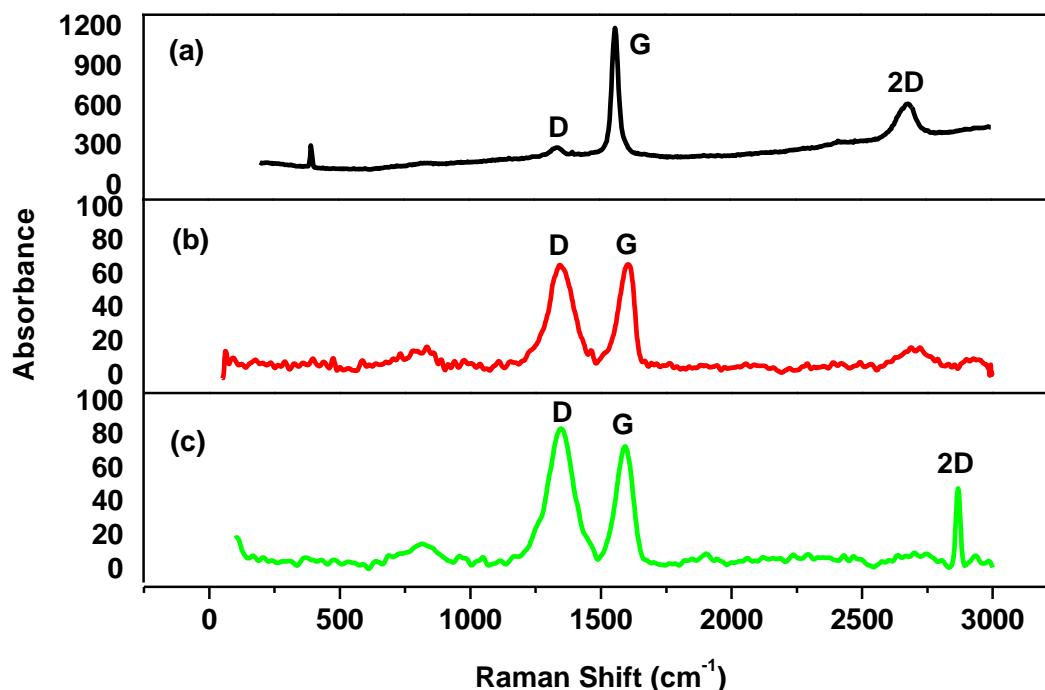


Figure 3.2. Raman spectra of (a) Graphite, (b) Graphene Oxide and (c) Graphene.

3.1.3. High Resolution Transmission Electron Microscopy (HRTEM)

Samples for HRTEM analysis were prepared by ultrasonication in pure ethanol and then drop-casted onto Cu grids. Highly ordered graphite, represented in Figure 3.3(a), shows dark flakes with straight edges due to the crystalline nature of pure graphite. Graphene oxide in Figure 3.3(b) is observed as crumpled transparent sheets having many wrinkles and folds while the HRTEM image of graphene in Figure 3.3(c) show similar microscopic features to GO but with fewer wrinkles and folds. Moreover, the variation in transparency of graphene indicates the variation in the number of graphene sheets stacked on each other hence, a decrease in transparency implies fewer stacked graphene sheets. At higher magnification in Figure 3.3(d), the exfoliation into individual sheets (indicated by arrows) is observed.

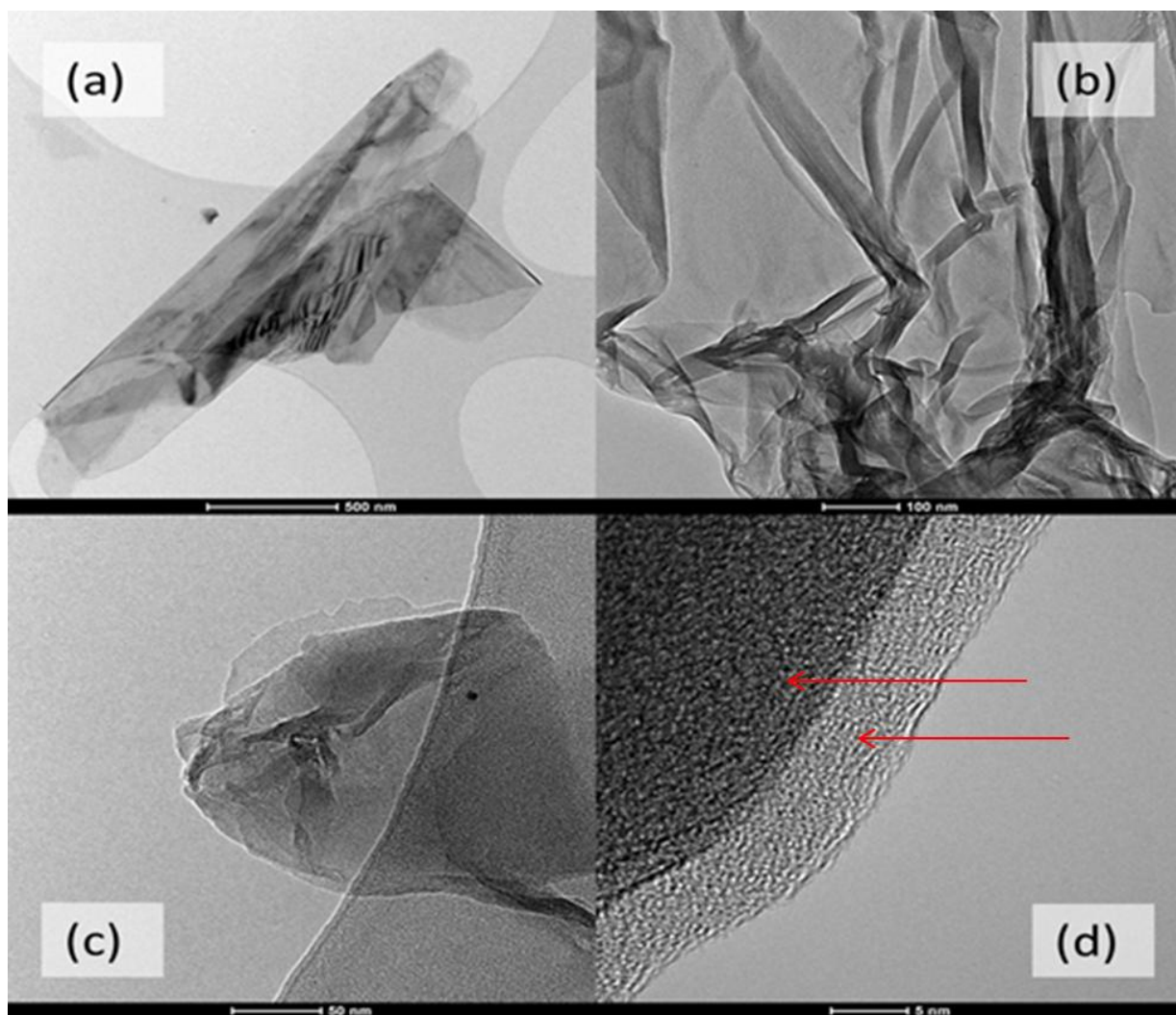


Figure 3.3. HRTEM images showing selected features of Graphite (a), Graphene Oxide (b) and Graphene (c) and (d).

3.2. Nafion-Graphene Pencil Graphite Bismuth-film Electrode Preparation (Electrode Coating Methods)

Various coating techniques were investigated for the preparation of the NG-PG-BiE namely, dip coating (with and without electrode pre-treatment), passive adsorption and electrodeposition. In the passive adsorption method (Figure 3.4(a)), electrodes were immersed in Nafion-graphene solutions in a DMF solvent for 1 hour to allow for adsorption to take place. The modified electrodes showed no enhancement in stripping peak currents indicating that no adsorption of the NG nanocomposite occurred. Electrochemical deposition (Figure 3.4(b)) provided enhanced sensitivity with graphene modification compared to the PG-BiE as discussed in our previous work [34]. Figure 3.4(b) shows the effect of the dip-coating method] and, similar to the passive adsorption method, no significant enhancement in electrode signals was achieved with the NG-PG-BiE in comparison with the N-PG-BiE. The dip coating procedure with electrode pre-treatment (Figure 3.4(c)) was the most suitable. In this procedure each pencil graphite electrode was place in the blank supporting electrolyte (0.1 M

acetate buffer solution) and pretreated by applying a potential of +1.4 V for 30 s to the electrode without stirring. Pretreatment was performed to increase the hydrophilic properties of the electrode surface through the introduction of oxygenated functionalities as demonstrated in the work by Levent *et al* [35].

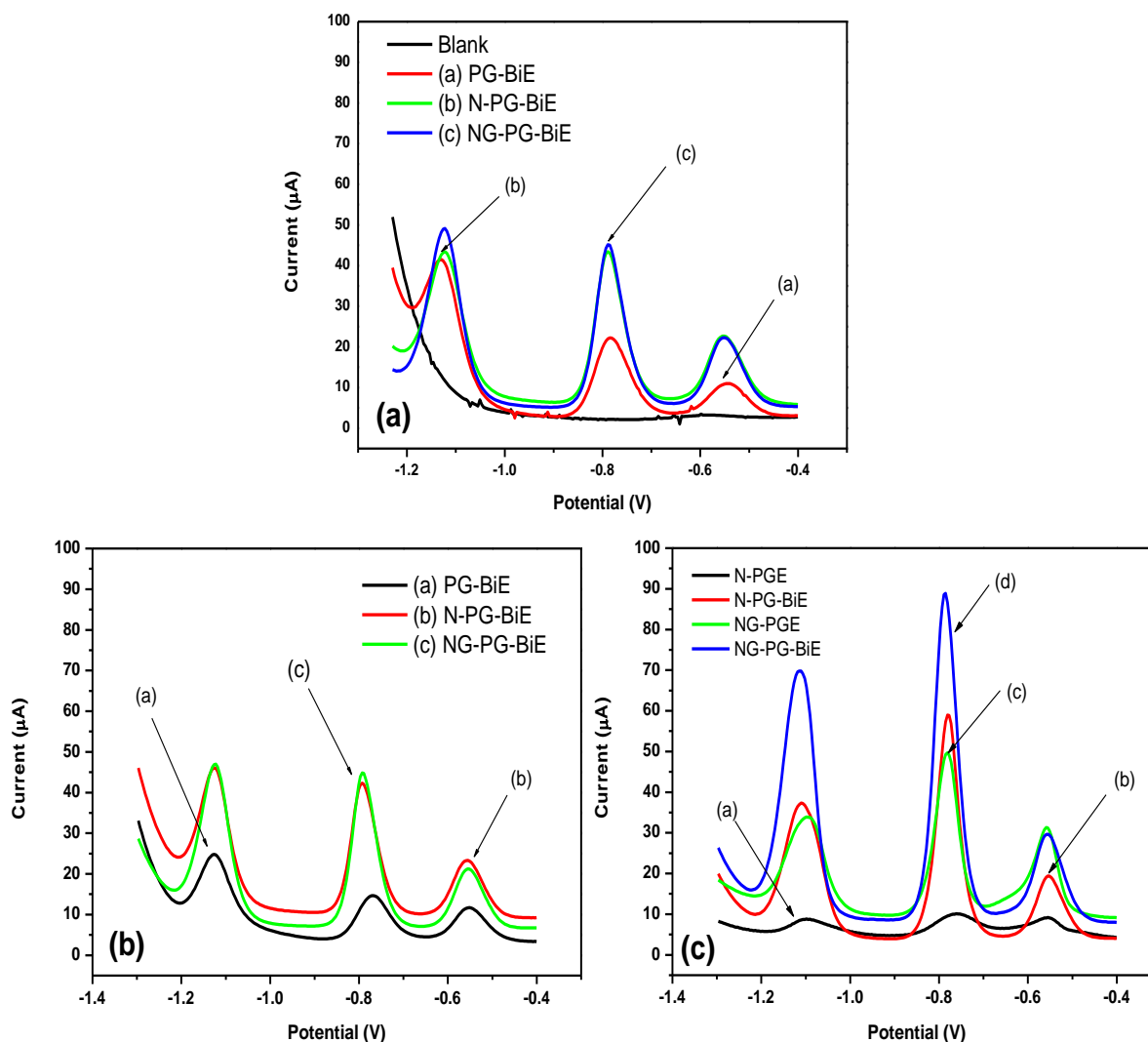


Figure 3.4. SWASV of Zn^{2+} , Cd^{2+} and Pb^{2+} at N-PG-BiE and NG-PG-BiE by a (a) passive adsorption method, (b) dip-coating method without electrode pre-treatment and (c) dip-coating method with electrochemical electrode pre-treatment. Supporting electrolyte: 0.1 M acetate buffer (pH 4.6), deposition potential (-1.4 V), deposition time (120 s), frequency (50 Hz), amplitude (0.025 V) and voltage step (0.005 V).

The pre-treated electrodes were then modified by dip-coating them into a solution containing a mixture of 0.2 % Nafion and 0.25 mg mL^{-1} graphene. A comparison of voltammograms of N-PG-BiE with NG-PG-BiE in Figure 3.4(c) shows that the modification of the N-PG-BiE with graphene to give the NG-PG-BiE gave larger stripping peak signals due to the enhanced surface-to-volume ratio and quantum confinement of the graphene nanosheets [45]. In addition, further peak signal enhancement is

achieved and sharper well-resolved stripping peak are obtained when using an *in situ* plated bismuth-film. This builds on the work done by Demetriades *et al.* who showed the enhancement in stripping peak currents at N-PG-BiEs compared to the bare pencil graphite electrodes [26]. Although the exact structure and morphology of Nafion is still in question today, however, the ion exchange property of Nafion is well known. Ion exchange takes place between the metal cations and the protons of the sulfonic group bringing a greater amount of metal ions closer to the electrode surface for reduction to form fused alloys with bismuth. The incorporation of graphene to form the Nafion-graphene nanocomposite allows for electron transfer through the thin Nafion-graphene nanocomposite film which is not possible for Nafion alone.

3.3. Film Stability and Reproducibility

The reproducibility of the NG-PG-BiE was performed by investigating the square wave voltammograms of three identical analyses. The stripping peak currents of $30 \mu\text{g L}^{-1}$ of Zn^{2+} , Cd^{2+} and Pb^{2+} at the NG-PG-BiE were identical with a relative standard deviation of 1.5 – 3.3 % for all target metal ions. Good reproducibility during electrode modification and analysis was thus achieved.

3.4. Effect of Supporting Electrolyte and Characteristic oxidation potentials of Bi^{3+} and target metal ions (Zn^{2+} , Cd^{2+} , and Pb^{2+})

The supporting electrolyte which is usually an acid [46] or acid buffer solution [47] is pivotal to the formation of well-resolved peaks and accurate quantitation. The electrochemical responses of the NG-PG-BiE towards the target metal ions in different electrolyte solutions namely, 0.1 M acetate buffer (pH 4.6), 0.1 M HCl solution (pH 2) and 0.1 M phosphate buffer (pH 7.1) were investigated and are shown in Figure 3.5.

In a 0.1 M HCl (pH 2.1) solution relatively small, broad peaks were observed for Cd^{2+} whereas the Pb^{2+} peaks are slightly taller. The hydrogen evolution severely distorts the Zn^{2+} signal to the extent that no well-defined peak was observed. On the other hand the stripping peaks recorded in phosphate buffer (0.1 M, pH 7.1) showed small, resolved peaks for Zn^{2+} and Pb^{2+} but, a taller Cd^{2+} peak. However, well-defined oxidative stripping peaks with no inter-metallic interferences and good resolution were observed at -1.1, -0.75, -0.50 and -0.06 V for Zn^{2+} , Cd^{2+} , Pb^{2+} and Bi^{3+} respectively, in acetate buffer solution (0.1 M, pH 4.6).

These results confirm the strong influence of electrolyte solution in anodic stripping voltammetric analysis.

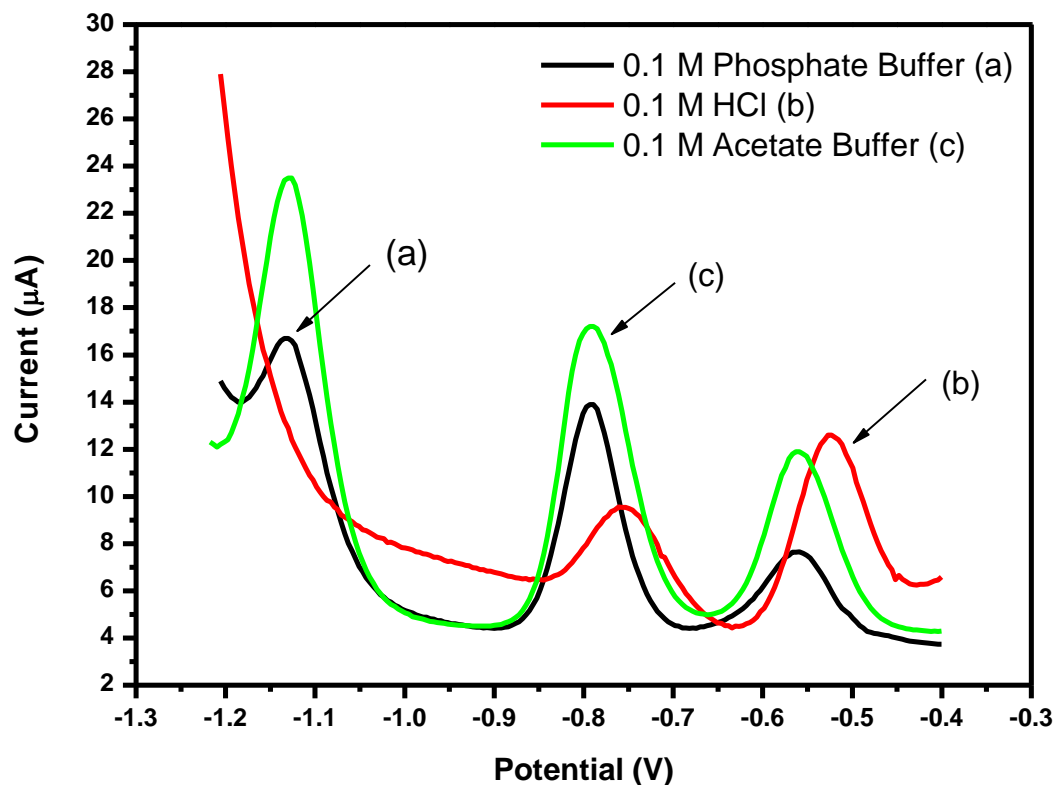


Figure 3.5. SWASV of $30 \mu\text{g L}^{-1}$ of Zn^{2+} , Cd^{2+} and Pb^{2+} at NG-PG-BiE with supporting electrolyte: (a) 0.1 M phosphate buffer (pH 7.1), (b) 0.1 M HCl and (c) 0.1 M acetate buffer (pH 4.6). Deposition potential: -1.4 V; deposition time: 120 s; frequency: 50 Hz; amplitude: 0.025 V and voltage step: 0.005 V.

3.5. Effect of the bismuth ion (Bi^{3+}) concentration

The procedure for depositing a bismuth film onto an electrode substrate is crucial since, film thickness greatly influences the performance bismuth film electrode (BiE) [48].

Bismuth–film electrodes (BiEs) are prepared either by *in situ* or *ex situ* electroplating of a bismuth film onto the surface of a conductive support. *In situ* plating is only suitable for the analysis of trace metals by anodic stripping voltammetry which involves cathodic electrolysis step [49]. The effect of bismuth ion concentration on the stripping responses of Zn^{2+} , Cd^{2+} and Pb^{2+} at Nafion-graphene pencil graphite electrodes (NG-PGE) is shown in Figure 3.6; here the Bi^{3+} concentrations were varied from 200 to 4000 $\mu\text{g L}^{-1}$. For all three target metal ions, similar increasing stripping currents were observed up to 800 $\mu\text{g L}^{-1}$ after which the currents significantly decreased for Cd^{2+} and Pb^{2+} but starts to level off at 4000 $\mu\text{g L}^{-1}$ for Zn^{2+} . Film thickness which is a consequence of Bi^{3+} ion concentration [26] results in the saturation of the electrode surface and causes a decrease in currents between 1000 and 5000 $\mu\text{g L}^{-1}$. A comparison of *in situ* and *ex situ* plating did not offer any major difference in peak

heights however, *in situ* plating simplifies the analysis and shortens analysis time [48] henceforth, $800 \mu\text{g L}^{-1}$ was selected for all future experiments.

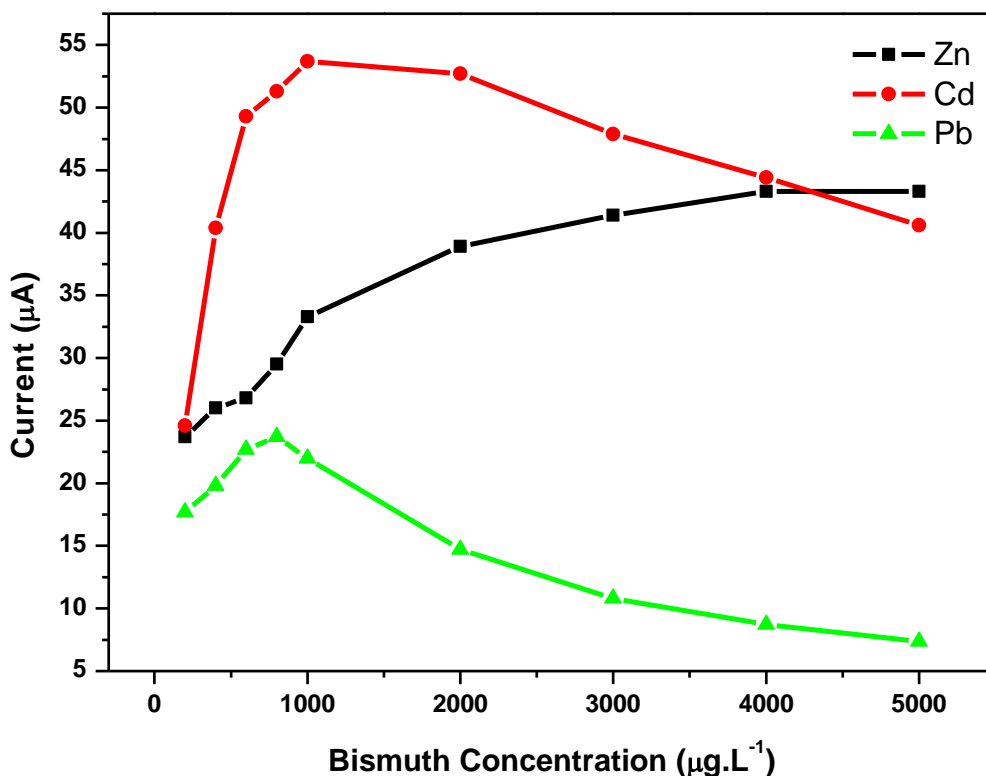


Figure 3.6. Effect of bismuth ion concentration on the stripping peak current of Zn^{2+} , Cd^{2+} and Pb^{2+} at Nafion-graphene pencil graphite bismuth film electrode (NG-PG-BiE) in a 0.1 M acetate buffer solution (pH 4.6) containing $20 \mu\text{g L}^{-1}$ of each metal.

3.6. Microscopic Characterisation of Nafion Graphene Modified Pencil Graphite Electrode (NG-PGE)

High resolution scanning electron microscopy (HRSEM) images of the bare PGE and NG-PGE surface morphologies are shown in Figure 3.7. The bare PGE surface shows surface roughness with grooves along the surface formed during the manufacturing process, Figures 3.7(a) and 3.7(b). Modification with a Nafion-graphene nanocomposite was interrogated under various magnifications in Figure 3.7(c) and 3.7(d). A thin sheet of Nafion-graphene is observed at the electrode surface confirming modification of the PGE with graphene sheets. Similar results are shown in work by Erdem *et al.* [50]. In addition, the presence of a Nafion-graphene nanocomposite coating is supported by the enhanced voltammetric signals in Figure 3.4(c).

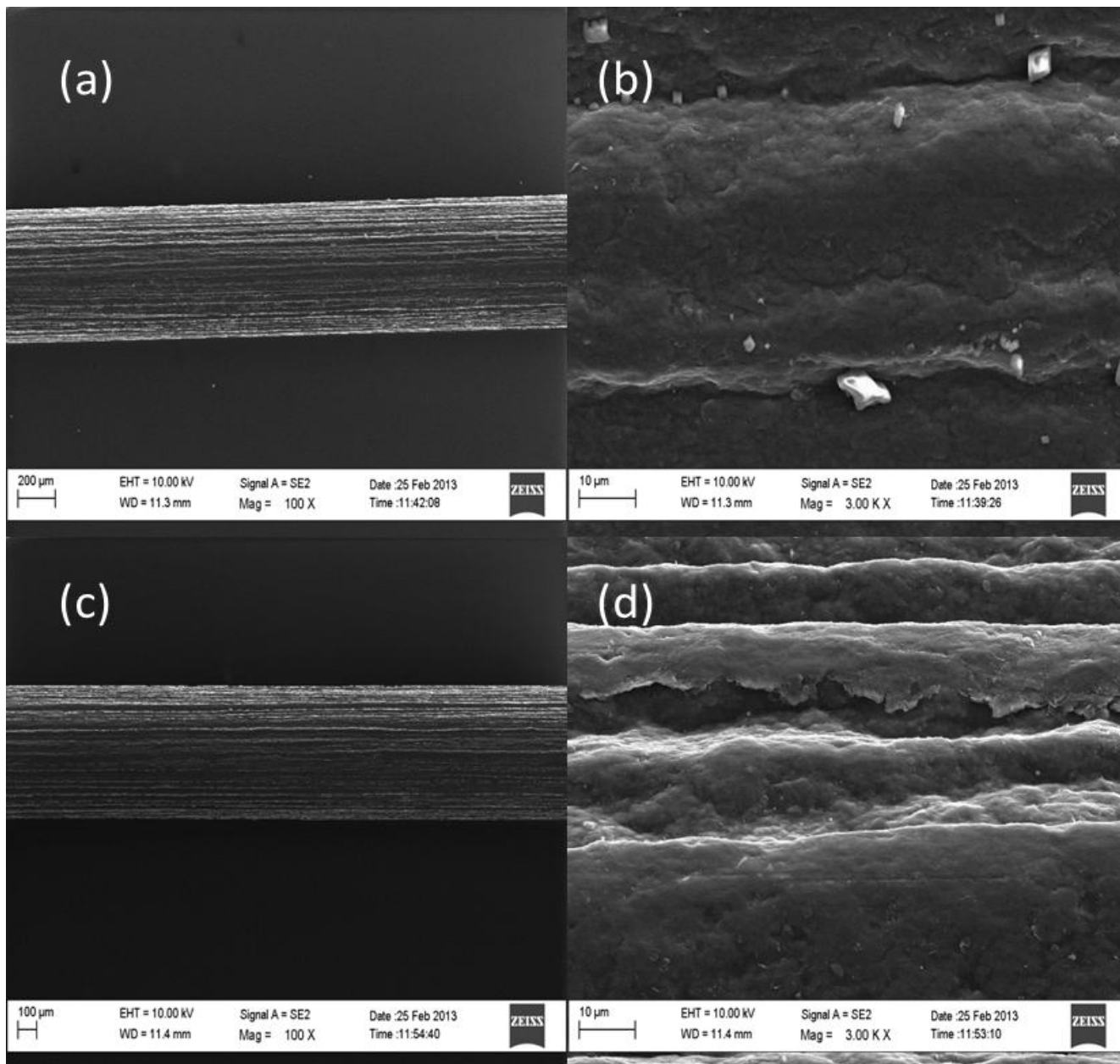


Figure 3.7. HRSEM images of bare PGEs (a) 100 times magnification, (b) 3000 times magnification and Nafion-graphene PGEs (c) 100 times magnification, (d) 3000 times magnification.

3.7. Optimisation of Instrumental Parameters at NG-PG-BiE

Optimisation of the square-wave instrumental parameters namely, amplitude, deposition potential, deposition time, frequency and rotation speed at the NG-PG-BiE were performed and shown in Figure 3.8.

Interrogation of stripping peak currents of target metal ions as a function of amplitude was performed in the range of 10 to 100 mV and shown in Figure 3.8(a). A general increase in peak current is observed with increasing amplitude.

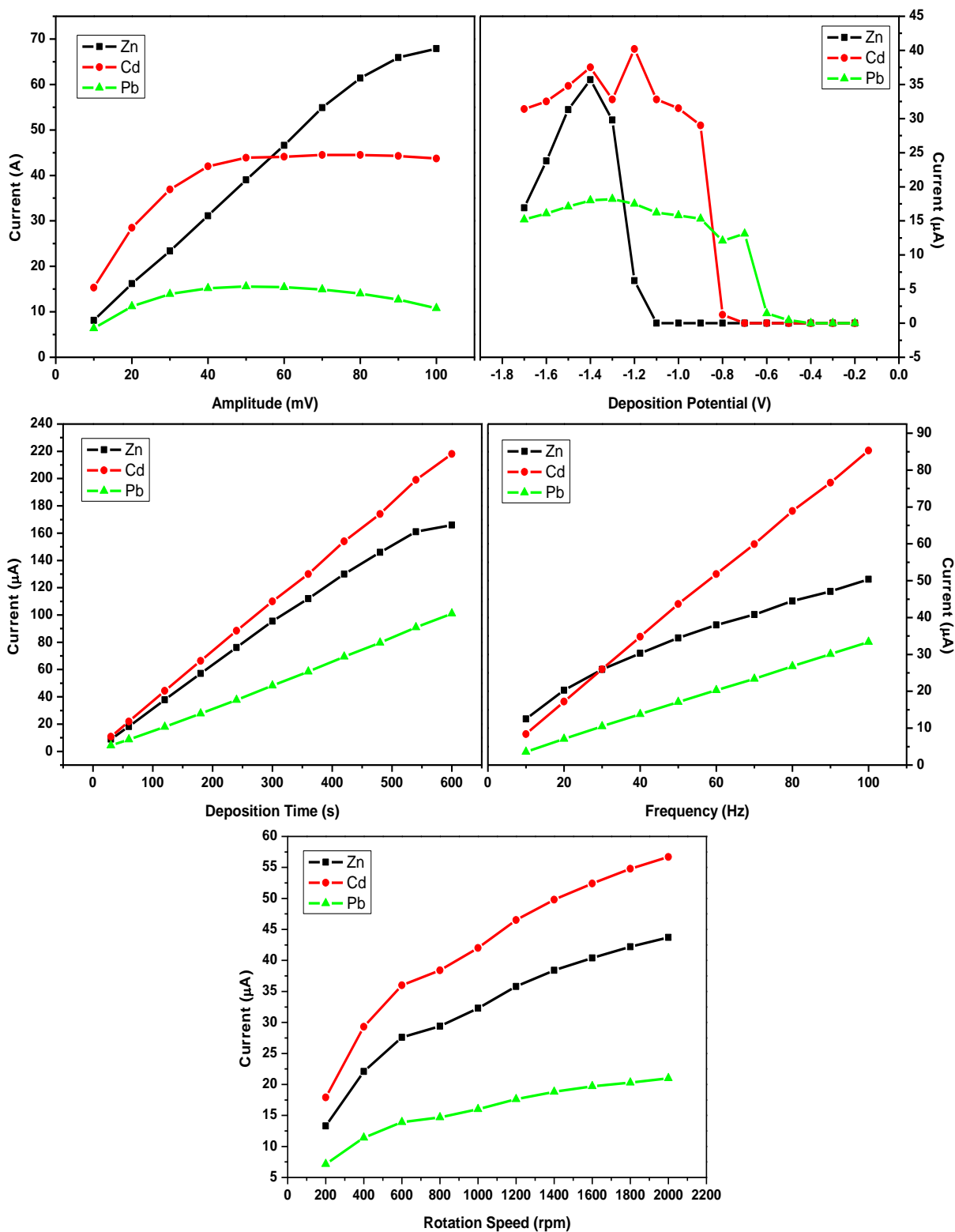


Figure 3.8. Effect of amplitude (a), deposition potential (b), deposition time (c), frequency (d) and rotation speed (e) on the stripping peak current of Zn^{2+} , Cd^{2+} and Pb^{2+} at Nafion-graphene pencil graphite bismuth film electrode (NG-PG-BiE) in a 0.1 M acetate buffer solution (pH 4.6) containing $20 \mu\text{g L}^{-1}$ of each metal and $800 \mu\text{g L}^{-1}$ of bismuth.

Cadmium and zinc show steeper rising slopes demonstrating their enhanced dependence on amplitude. Lead however, increases to a maximum of 60 mV before stabilizing. An amplitude of 40 mV was selected for subsequent experiments based on the information that any further amplitude increases does not result in a significant increase in peak current.

The deposition step, which governs the loading of metal ions onto the working electrode, is a crucial step in any form of stripping analysis. An investigation of the effect of deposition potential on the peak currents of Zn^{2+} , Cd^{2+} and Pb^{2+} at the NG-PG-BiE is demonstrated in Figure 3.8(b). The potential was studied in the range from +0.2 V to -1.7 V.

The stripping peak currents of all three metal ions increased with increasing negative potentials as the characteristic redox potentials of the ions was reached. Maximum stripping peak currents were observed at -1.4 V for all ions of interest at the BiE since, preferential reduction and deposition of metal ions at the electrode surface occur at this potential.

Electrode saturation occurs at values more negative than -1.4 V after which the peak currents continuously decreases hence, a deposition potential of -1.4 V was selected as the optimum deposition potential in further analyses.

The influence of deposition time on the stripping peak currents of Zn^{2+} , Cd^{2+} and Pb^{2+} on was investigated and is summarized in Figure 3.8(c). The peak currents for all three metal ions increased linearly with increasing deposition times from 30 to 600 seconds thus, a deposition time of 120 seconds was selected in order to limit the total analysis time. Figure 3.8(d) shows the dependence of peak currents on the square wave frequency in the 12.5 Hz to 125 Hz range. Increasing the frequency showed increased peak currents as a result of increased scan rate [51]. A frequency of 50 Hz was chosen since distinct peaks with good resolution were obtained.

Rotation speed which facilitates the movement of free metal ions from the bulk solution to the electrode surface during the pre-concentration step was studied. Figure 3.8(e) shows that with increasing rotation speed from 200 to 2000 rpm, the stripping peak currents of all three target metal ions increased hence, a rotation speed of 1000 rpm was selected for further analyses.

3.8. Analytical Performance of Nafion-Graphene modified Pencil Graphite Bismuth-film Electrodes (NG-PG-BiEs)

Figure 3.9 and 3.10 below, show square-wave anodic stripping voltammograms and their corresponding calibration plots for the simultaneous and individual analysis of Zn^{2+} , Cd^{2+} and Pb^{2+} in 0.1 M acetate buffer solution (pH 4.6) at NG-PG-BiE. Two concentration ranges, namely: 2 – 20 $\mu g L^{-1}$ and 10 – 100 $\mu g L^{-1}$ were used to investigate the analytical performance of the NG-PG-BiE. Well-defined, sharp peaks were observed for all target metal ions with a slight positive shift due to oxidation of the metals becoming less reversible [51].

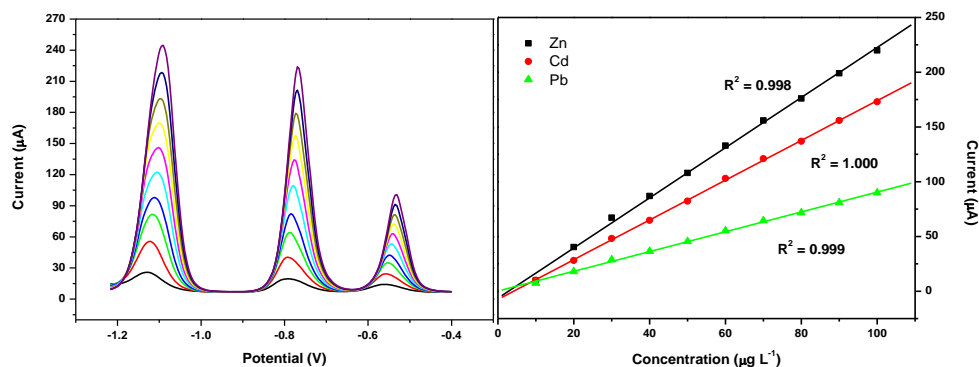


Figure 3.9. SWASV and corresponding calibration plots of simultaneous analysis of Zn²⁺, Cd²⁺ and Pb²⁺ obtained at NG-PG-BiE over 10 – 100 μg L⁻¹. Supporting electrolyte: 0.1 M acetate buffer (pH 4.6), deposition time: 120, deposition potential: -1.4 V, rotation speed: 1000 rpm, frequency: 50 Hz, amplitude: 0.04 V and sweep rate: 0.2975 V. s⁻¹.

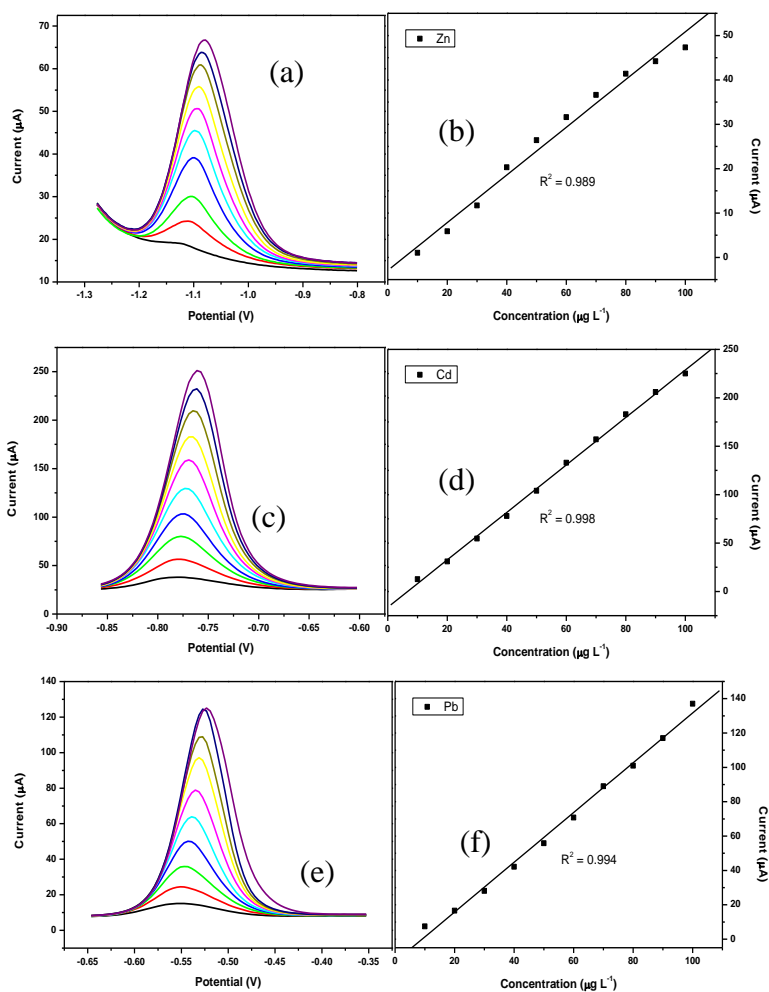


Figure 3.10. SWASV and corresponding calibration plots for individual analysis of (a and b) Zn²⁺, (c and d) Cd²⁺ and (e and f) Pb²⁺ obtained at NG-PG-BiE over 10 – 100 μg L⁻¹. Supporting electrolyte: 0.1 M acetate buffer (pH 4.6), deposition time (120), deposition potential (-1.4 V), rotation speed (1000 rpm), frequency (50 Hz), amplitude (0.04 V) and sweep rate (0.2975 V s⁻¹).

Detection limits for the metal ions of interest were determined using the following equation;

$$D.L. = \frac{3\sigma}{\text{slope}}$$

- Where, D.L; is the limit of detection
- 3σ; is three times the standard deviation of the blanks
- Slope; is the gradient (slope) of the calibration curve

The standard deviation of the blanks was calculated based on ten replications of the electrode’s response in the electrolyte solution. Table 3.1 summarises detection limits obtained for the simultaneous and individual analysis carried out at a deposition time of 120 s over two concentration ranges namely, 2 -20 μg L⁻¹ and 10 – 100 μg L⁻¹. The calculated detection limits for Zn²⁺, Cd²⁺ and Pb²⁺ were 0.224 μg L⁻¹, 0.098 μg L⁻¹ and 0.204 μg L⁻¹ for simultaneous analysis while individual analysis gave detection limits of 0.167 μg L⁻¹, 0.098 μg L⁻¹ and 0.125 μg L⁻¹ for Zn²⁺, Cd²⁺ and Pb²⁺ respectively. Furthermore, the improved detection limits observed for individual analysis above simultaneous analysis is due to the lack of competition for available sites at the electrode surface. A comparison of detection limits with other previously reported bismuth-film electrodes are tabulated in Table 3.2 and shows that the NG-PG-BiE compares well with the electrodes in this table when a deposition time of 120 seconds is used.

Table 3.1. Calibration data representing Simultaneous and Individual Analysis of Zn²⁺, Cd²⁺ and Pb²⁺ at NG-PG-BiEs in 0.1 M acetate buffer solution (pH 4.6) at 120s.

Analytical Parameter	Simultaneous Analysis (2 – 20 μg L ⁻¹)			Individual Analysis (2 – 20 μg L ⁻¹)		
	Zn ²⁺	Cd ²⁺	Pb ²⁺	Zn ²⁺	Cd ²⁺	Pb ²⁺
Sensitivity (μA L μg ⁻¹)	2.08 (±0.113)	1.89 (±0.071)	0.992 (±0.064)	0.432 (±0.021)	1.61 (±0.017)	0.747 (±0.032)
Correlation Coefficient (R ²)	0.989	0.998	0.993	0.998	0.995	0.989
Detection Limits (μg L ⁻¹)	0.257 (±0.032)	0.098 (±0.017)	0.204 (±0.009)	0.167 (±0.028)	0.151 (±0.004)	0.125 (±0.013)
Analytical Parameter	Simultaneous Analysis (10 – 100 μg L ⁻¹)			Individual Analysis (10 – 100 μg L ⁻¹)		
	Zn ²⁺	Cd ²⁺	Pb ²⁺	Zn ²⁺	Cd ²⁺	Pb ²⁺
Sensitivity (μA L μg ⁻¹)	2.29 (±0.021)	1.82 (±0.037)	0.904 (±0.019)	0.531 (±0.005)	2.431 (±0.035)	1.457 (±0.029)
Correlation Coefficient (R ²)	0.998	1.000	0.999	0.990	0.998	0.994
Detection Limits (μg L ⁻¹)	0.224 (±0.021)	0.099 (±0.006)	0.177 (±0.022)	0.168 (±0.005)	0.098 (±0.005)	0.141 (±0.001)

Table 3.2. A selected summary of previously reported detection limits for Zn^{2+} , Cd^{2+} and Pb^{2+} at various Bismuth-film electrodes (BiFE)

Metals Detected	Electrode Substrate	Measurement Technique	Deposition Time (s)	Detection Limit ($\mu g L^{-1}$)	Reference
Pb^{2+} , Cd^{2+}	Nafion-G BiFE	DPASV	300	$Pb^{2+} = 0.02$ $Cd^{2+} = 0.02$	[3]
Pb^{2+} , Cd^{2+} , Zn^{2+}	BiF-PGE	SWASV	120	$Pb^{2+} = 0.40$ $Cd^{2+} = 0.30$ $Zn^{2+} = 0.40$	[26]
Pb^{2+} , Cd^{2+} , Zn^{2+}	ERGO-PG-BiE	SWASV	120	$Pb^{2+} = 0.12$ $Cd^{2+} = 0.09$ $Zn^{2+} = 0.19$	[34]
Pb^{2+} , Cd^{2+} , Zn^{2+}	NC(Bpy)BiFE	SWASV	120	$Pb^{2+} = 0.08$ $Cd^{2+} = 0.12$	[52]
Pb^{2+} , Cd^{2+}	Bi film C-paste	SWASV	120	$Pb^{2+} = 0.80$ $Cd^{2+} = 1.00$	[53]
Pb^{2+} , Cd^{2+}	Bi/GNFs-Nafion/GCE	DPASV	300	$Pb^{2+} = 0.02$ $Cd^{2+} = 0.09$	[29]
Pb^{2+} , Cd^{2+} , Zn^{2+}	Bi-CNT/GCE	SWASV	300	$Pb^{2+} = 1.30$ $Cd^{2+} = 0.70$ $Zn^{2+} = 12.0$	[28]
Pb^{2+} , Cd^{2+}	Bi nanopowder on carbon	SWASV	180	$Pb^{2+} = 0.15$ $Cd^{2+} = 0.07$	[54]
Pb^{2+} , Cd^{2+} , Zn^{2+} Simultaneous Analysis	NG-PG-BiE	SWASV	120	$Pb^{2+} = 0.22$ $Cd^{2+} = 0.09$ $Zn^{2+} = 0.20$	This Work
Pb^{2+} , Cd^{2+} , Zn^{2+} Individual Analysis	NG-PG-BiE	SWASV	120	$Pb^{2+} = 0.17$ $Cd^{2+} = 0.09$ $Zn^{2+} = 0.13$	This Work

3.9. Recovery Studies of NG-PG-BiE

The NG-PG-BiE was used in recovery studies to determine the target metal ions in test solutions. Known concentrations of target metal ions were used to spike 10 mL portions of 0.1 M acetate buffer solutions followed by their determination using the standard addition method (Figure 3.11). An advantage of this method is that it compensates for interferences caused by the sample matrix. Recovery percentages of the metal ions from test solutions spiked with $30 \mu g L^{-1}$ Zn^{2+} , Cd^{2+} and Pb^{2+} yielded recovery values of 77.56 %, 94.35 % and 92.83 % for simultaneous analysis while for individual analysis the recovery values were 97.36 %, 99.24 % and 97.62 % for Zn^{2+} , Cd^{2+} and Pb^{2+} respectively. The percentage recoveries for simultaneous and individual analyses in Table 3.3 show slightly higher recovery percentages were obtained for individual analysis due to the lack of competition for available sites at the electrode surface.

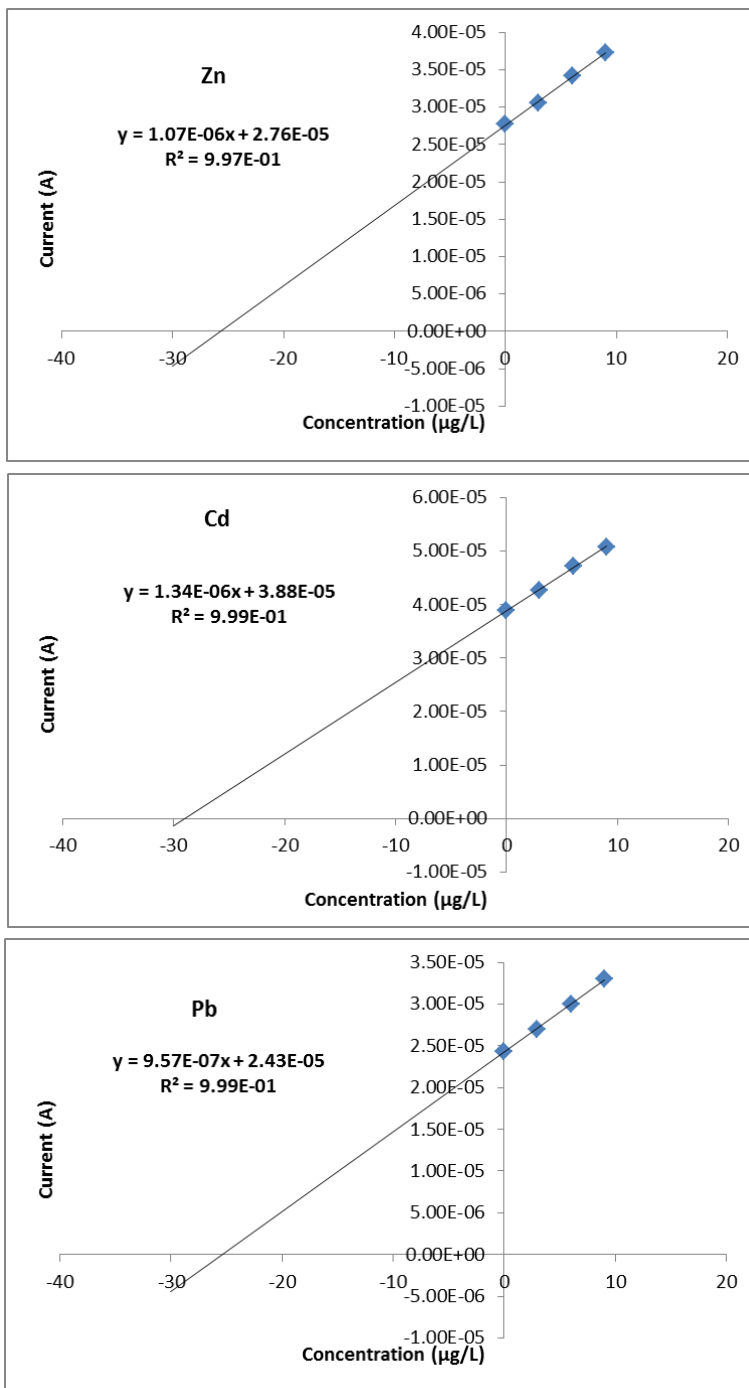


Figure 3.11. Standard Addition plots for the simultaneous determination of (a) Zn²⁺, (b) Cd²⁺ and (c) Pb²⁺ at NG-PG-BiE in test solutions.

Table 3.3. Recovery data for the simultaneous and individual determination of Zn²⁺, Cd²⁺ and Pb²⁺ at NG-PG-BiEs in test solutions

Recovery Studies of Zn ²⁺ , Cd ²⁺ and Pb ²⁺ in Test Solutions			
Simultaneous Analysis			
	Zn ²⁺	Cd ²⁺	Pb ²⁺
Original (µg L ⁻¹)	ND	ND	ND
Added (µg L ⁻¹)	30	30	30

Found ($\mu\text{g L}^{-1}$)	23.27	28.31	27.85
RSD (%)	2.89	3.74	4.21
Recovery (%)	77.56	94.35	92.83
Individual Analysis			
	Zn ²⁺	Cd ²⁺	Pb ²⁺
Original ($\mu\text{g L}^{-1}$)	ND	ND	ND
Added ($\mu\text{g L}^{-1}$)	30	30	30
Found ($\mu\text{g L}^{-1}$)	29.21	29.77	29.29
RSD (%)	3.17	2.81	3.75
Recovery (%)	97.36	99.24	97.62

3.10. Application to Tap Water Samples

The NG-PG-BiE developed was employed as an electrochemical sensing platform for the analysis of tap water samples. Tap water were collected in our laboratory and analysed for Zn²⁺, Cd²⁺ and Pb²⁺ using the standard addition method. None of the target metal ions were detected at a pre-concentration time of 120 seconds during either simultaneous or individual analyses due to their low concentrations. However, spiking tap water samples with 5 $\mu\text{g L}^{-1}$, 20 $\mu\text{g L}^{-1}$ and 30 $\mu\text{g L}^{-1}$ of the target metal ions respectively, yielded good recoveries as shown in Table 3.4. Increasing concentrations from 5 $\mu\text{g L}^{-1}$ to 20 $\mu\text{g L}^{-1}$ and then to 30 $\mu\text{g L}^{-1}$ as well as, performing individual analysis improved the percentage recoveries for all three metal ions. The lower recoveries for Zn²⁺ can be largely attributed to errors arising from the distortion of the zinc oxidation peak current caused by hydrogen gas evolution. The lower recoveries obtained for tap water samples spiked with 5 $\mu\text{g L}^{-1}$ can be attributed to the fact that errors are generally greater when working closer at the detection limits of the metal ions [51].

Table 3.4. Recovery percentages for Zn²⁺, Cd²⁺, and Pb²⁺, at the NG-PG-BiE in tap water samples using a deposition time of 120 seconds.

Simultaneous Analysis					
Metal Ion	Original ($\mu\text{g L}^{-1}$)	Added ($\mu\text{g L}^{-1}$)	Found ($\mu\text{g L}^{-1}$)	RSD (%)	Recovery (%)
Zn ²⁺	ND	5	2.96	3.05	59.14
	ND	20	12.52	2.84	62.59
	ND	30	20.52	3.83	68.42
Cd ²⁺	ND	5	4.34	5.12	86.74
	ND	20	18.03	5.43	90.14
	ND	30	30.73	4.19	102.43
Pb ²⁺	ND	5	4.48	2.78	89.61
	ND	20	18.69	5.36	93.47
	ND	30	29.44	1.46	98.12
Individual Analysis					
Metal Ion	Original ($\mu\text{g L}^{-1}$)	Added ($\mu\text{g L}^{-1}$)	Found ($\mu\text{g L}^{-1}$)	RSD (%)	Recovery (%)
Zn ²⁺	ND	5	4.14	4.61	82.84
	ND	20	17.84	5.77	89.23

Cd ²⁺	ND	30	28.60	2.38	95.34
	ND	5	4.02	3.54	80.36
	ND	20	17.29	4.85	86.45
Pb ²⁺	ND	30	29.94	1.22	99.79
	ND	5	4.62	2.21	92.47
	ND	20	20.30	1.11	101.51
	ND	30	29.53	2.84	98.43

n = 3, where n is number of repetitive cycles performed

ND, not detected

In order to meet the United States Environmental Protection Agency’s (USEPA) maximum contaminant level (MCL) for zinc (5 mg L⁻¹), cadmium (0.005 mg L⁻¹) and lead (0.015 mg L⁻¹) in drinking water, a longer deposition time of 360 seconds was used. Typical voltammograms obtained during the simultaneous analysis of heavy metal ions together with their corresponding standard addition curves is shown in Figure 3.12.

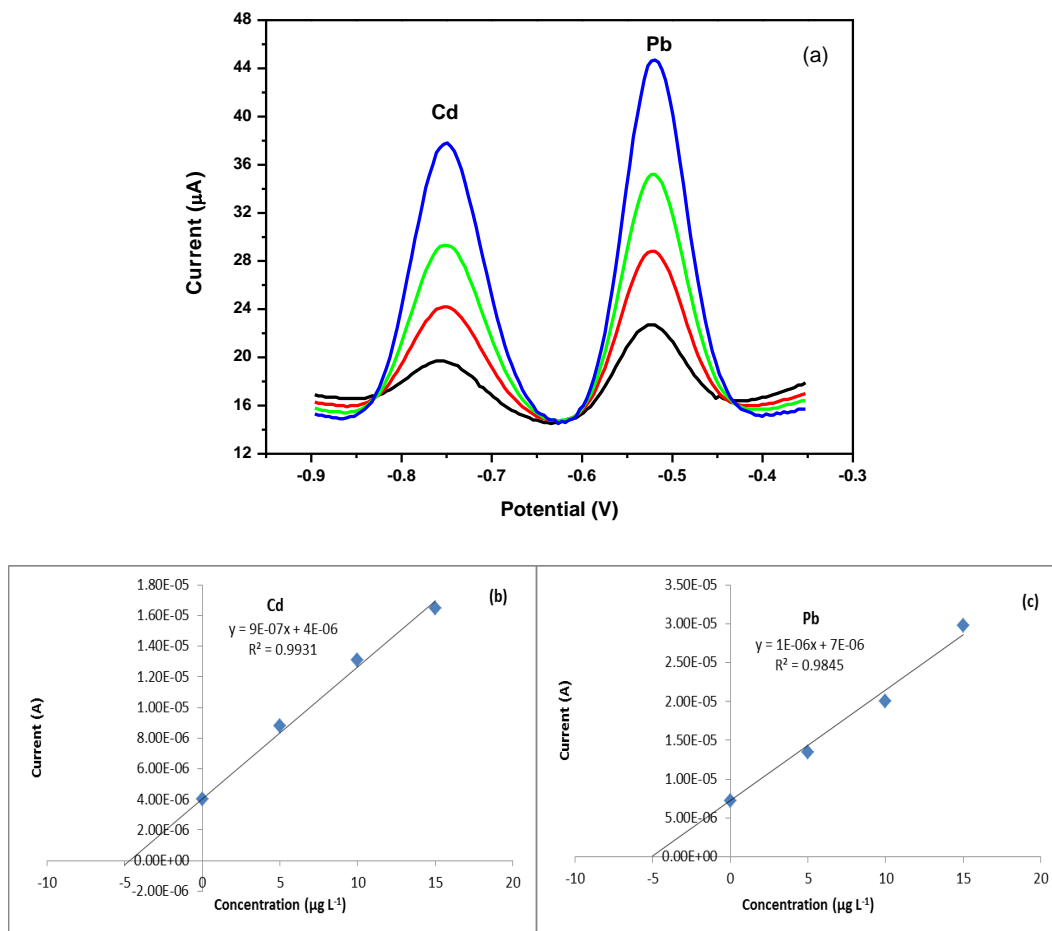


Figure 3.12. Square wave voltammograms (a) and corresponding standard addition calibration curves of Cd²⁺ (b) and (c) Pb²⁺ for the simultaneous analysis of tap water (pH 4.6) spiked with 5 µg L⁻¹ of each of metal ion using a deposition time of 360 seconds.

Table 3.5 shows the percentage recovery obtained when using a deposition time of 360 seconds during simultaneous and individual analysis. As expected, the longer pre-concentration time allows for more metal ions to be deposited at the electrode surface resulting in improved sensitivity.

Table 3.5. Recovery for the determination of Zn^{2+} , Cd^{2+} and Pb^{2+} in tap water samples using NG-PG-BiE at pre-concentration time of 360 seconds

Recovery for the determination of Zn^{2+} , Cd^{2+} and Pb^{2+} in tap water samples					
Simultaneous Analysis					
Metal Ion	Original ($\mu\text{g L}^{-1}$)	Added ($\mu\text{g L}^{-1}$)	Found ($\mu\text{g L}^{-1}$)	RSD (%)	Recovery (%)
Zn^{2+}	ND	5	ND	ND	ND
Cd^{2+}	ND	5	4.72	2.11	94.36
Pb^{2+}	ND	5	5.18	1.93	103.52
Individual Analysis					
Metal Ion	Original ($\mu\text{g L}^{-1}$)	Added ($\mu\text{g L}^{-1}$)	Found ($\mu\text{g L}^{-1}$)	RSD (%)	Recovery (%)
Zn^{2+}	ND	5	ND	ND	ND
Cd^{2+}	ND	5	5.08	1.90	101.68
Pb^{2+}	ND	5	4.95	1.87	98.91

$n = 3$, where n is number of repetitive cycles performed

ND, not detected

Recovery percentages summarised in Table 3.5 show improved recoveries for individual analysis at 102 % and 99 % for Cd^{2+} and Pb^{2+} respectively. The accurate quantitation of heavy metals at concentration below the USEPA standards proves the effective use of the NG-PG-BiE in conjunction with SWASV for detection of trace amounts of metals in drinking water.

4. CONCLUSIONS

Modification of pencil graphite electrodes with a Nafion-graphene nanocomposite followed by the *in situ* plated bismuth film resulted in an ultra-sensitive sensing platform (NG-PG-BiE) for the detection of trace amounts of Zn^{2+} , Cd^{2+} and Pb^{2+} by square-wave anodic stripping voltammetry. The pre-treatment of pencil graphite prior to dip coating has shown to have a significant influence on the peak signals. Detection limits at values comparable to other known bismuth-film electrodes were attained and below the USEPA maximum contamination levels. In addition, the accurate detection of metal ions in drinking water with a 5 % error proved the enhanced sensing capabilities of the Nafion-graphene platform.

References

1. J. Wang, *Stripping Analysis-Principles, Instrumentation and Application*, VCH Publishers Deerfield Beach, FL, USA, Inc. (1985)
2. A. Ala, A. Walker, K. Ashkan, J. Dooley and M. Schilsky, *The Lancet*, 369 (2007) 397-408
3. J. Li, S. Guo, Y. Zhai and E. Wang, *Anal. Chim. Acta*, 649 (2009) 196-201
4. M.J. Goldcamp, M.N. Underwood, J. Cloud and S. Harshman, *J. Chem. Edu.*, 85 (2008)
5. B. Claux and O. Vittori, *Electroanalysis*, 21, 19 (2007) 2243-2246
6. G. Long, L. Freedman and G. Doak, *Encycl. Chem. Technol.*, (1978) 912-937
7. J. Wang, *Electroanalysis*, 17 (2005) 15-16.
8. F. Arduini, J. Calvo, G. Palleschi, D. Moscone, 29, 11 (2010) 1295-1304
9. R. Pauliukaite, S. Hocevar B. Ogorevc, and J. Wang, *Electroanalysis*, 16 (2004) 719
10. V. Guzsvany, H. Nakajima, N. Soh, K. Nakano and T. Imato, *Anal. Chim. Acta*, 658 (2010) 12-17
11. S. Hocevar, *Anal. Chem.*, 79 no. 22 (2007) 8639-8643
12. J. Wang, A. Kawde and E. Sahlin, *Analyst, The Royal Society of Chemistry*, 125 (2000) 5-7
13. A. Ozcan, Y. Sahin, *Biosens. Bioelectron.*, 25, 11 (2010) 2497-2502
14. M. Rahman and M. Won, Y. Shim, *Anal. Chem.*, 75 (2003) 1123-1129
15. L. Chen, Z. Li, Y. Meng, P. Zhang, Z. Su, Y. Liu, Y. Huang, Y. Zhou and Q. Xie, *Sensors and Actuators B: Chemical*, 191 (2014) 94-101
16. M. Imisides, R. John and P.Riley, G. Wallace, *Electroanalysis*, 3 (1991) 879-889
17. A. Bond, P. Mahona, J. Schiewe and V. Vicente-Beckett, *Anal. Chim. Acta*, 345 (1997) 67-74
18. G. Wilkes, M. Tant and K. Mauritz, *Ionomers: Synthesis, Structure, Properties and Elasticity*, Eds.; Chapman and Hall: London (1997)
19. S. Schlick, *Characterization, Theory and Applications*, CRC Press: Boca Raton, FL (1996)
20. M. Bass, A. Berman, A. Singh, O. Konovalov and V. Freger, *J. Phys. Chem.*, 114 (2010) 3784-3790
21. J. Wang, M. Musameh and Y. Lin, *J. Am. Chem. Soc.*, 125 (2003) 2408-2409
22. Y. Shao, J. Wang, H. Wu, J. Liu, I. Aksay and Y. Lin, *Electroanalysis*, 10 (2010) 1027-1036
23. M. Ahamed and M. Siddiqui, *Clin. Chim. Acta*, 383 (2007) 57-64
24. C. Willemse, K. Tlhomelang, N. Jahed, P. Baker and E. Iwuoha, *Sensors*, 11 (2011) 3970-3987
25. G. Kefala, A. Economou, A. Voulgaropoulos and M. Sofoniou, *Talanta*, 61 (2003) 603-610
26. D. Demetriades, A. Economou and A. Voulgaropoulos, *Anal. Chim. Acta*, 519 (2004) 167-172
27. H. Xu, L. Zeng, S. Xing, Y. Xian, G. Shi and L. Jin, *Electroanalysis*, 24, 20 (2008) 2655-2662
28. G. Hwang, W. Han, J. Park and S. Kang, *Talanta*, 76 (2008) 301-308
29. D. Li, J. Jia and J. Wang, *Talanta*, 83 (2010) 332-336
30. J. Gong, T. Zhou, D. Song and L. Zhang, *Sensors and Actuators B: Chemical*, 150, 2 (2010) 491-497
31. S. Zbeda, K. Pokpas, S. Titinchi, N. Jahed, P. Baker and E. Iwuoha, *Int. J. Electrochem. Sci.*, 8 (2013) 11125-11141
32. J. Li, S. Guo, Y. Zhai, E. Wang, *Electrochem. Comm.*, 11, 5 (2009) 1085-1088
33. W. Hummers and R. Offeman, *J. Anal. Chem. Soc.*, 1339 (1958)
34. K. Pokpas, S. Zbeda, N. Mohammed, N. Jahed, P. Baker and E. Iwuoha, *Int. J. Electrochem. Sci.*, 9 (2014) 736-759
35. A. Levent and Y. Yardim, Z. Sentruk, *Electrochim. Acta*, 55 (2009) 190-195
36. D. Marcano, D. Kosynkin, J. Berlin, A. Sinitskii, Z. Sun, A. Slesarev, L. Alemany, W. Lu, J. Tour, *ACS Nano*, 4, 8 (2010) 4806-4814
37. W. Chen and L. Yan, *Nanoscale*, 2 (2010) 559-563
38. A. Bourlinos, D. Gournis, D. Petridis, T. Szabo, A. Szeri and I. Dekany, *Langmuir*, 19 (2003) 6050-6055
39. S. Stankovich, D. Dikin, R. Piner, K. Kohlhaas, A. Kleinhammes, Y. Jia, Y. Wu, S. Nguyen and R. Ruoff, *Carbon*, (2007) 1558-1565

40. A. Eckmann, A. Felten, A. Mishchenko, L. Britnell, R. Krupke, K. Noveslov, C. Casiraghi, *ACS Nano*, 12 (2012) 3925-3930
41. Y. Zhu, S. Murali, W. Cai, X. Li, J. Won Suk, J.R. Potts, R.S. Ruoff, *Adv. Mater.*, 22 (2010) 3906-3924
42. J. Shen, Y. Hu, M. Shi, X. Lu, C. Qin, C. Li and M. Ye, *Chem. Mater.*, 21 (2009) 3514-3520
43. V. Singh, D. Joung, L. Zhai, S. Das and S. Khondaker, S. Seal, *Science*, 56 (2011) 1178-1271
44. Y. Zhu, *J. Chem. Soc.*, 132 (2010) 1227-1233
45. J. Allen, V. Tung and R. Kaner, *Chem. Rev.*, 110 (2010) 132-146
46. H. Sopha, S. Hocevar, B. Pihlar and B. Ogorevc, *Electrochim. Acta*, 60 (2012) 274-277
47. K. Asadpour-Zeynali and P. Najafi-Marandi, *Electroanalysis*, 23, 9 (2011) 2241-2247
48. A. Economou, *Trends in Anal. Chem.*, 24, 4 (2005) 334-340
49. N. Lezi, V. Vyskocil and A. Economou, J. Barek, *Sensing in Electroanalysis*, (2012) 71-78
50. A. Erdem, H. Karadeniz and A. Caliskan, *Electroanalysis*, 21 (2009) 464-471
51. W. Yi, Y. Li, G. Ran, H. Luo and N. Li, *Microchim. Acta*, 179 (2012) 171-177
52. F. Torma, M. Kadar, K. Toth and E. Tatar, *Anal. Chim. Acta*, 619 (2008) 173-182
53. I. Svancara, L. Baldrianova, E. Tesarova, S. Hocevar, S. Elsuccary, A. Economou, S. Sotiropoulos, Ogorevc. and K. B. Vytras, *Electroanalysis*, 18 (2006) 177
54. G. Lee, H. Lee and C. Rhee, *Electrochem. Comm.*, 9 (2007) 2514-2518

© 2014 The Authors. Published by ESG (www.electrochemsci.org). This article is an open access article distributed under the terms and conditions of the Creative Commons Attribution license (<http://creativecommons.org/licenses/by/4.0/>).